

$$F(\phi) = 1 - \frac{16}{7}\phi^{1/2} + \frac{4}{3}\phi - \frac{1}{21}\phi^4 \quad (5.6.15)$$

$$\phi = \frac{2\tau_y}{ac} \quad (5.6.16)$$

Hastighetsprofilen over kartverrsnittet blir omrent som for Bingham-fluiden i fig. 5.12.

For $\tau_y = 0$, går Casson-fluiden over til å bli en Newton-fluid. Formlene (5.6.11-14) reduseres nå til

$$r_p = 0, \quad v_p \equiv v_0 = \frac{ca^2}{4\mu} \quad (5.6.17)$$

$$v(R) = v_0 [1 - (R/a)^2] \quad (5.6.18)$$

$$Q = \frac{\pi a^4 c}{8\mu} = \frac{\pi d^4 c}{128\mu} \quad (5.6.19)$$

Den siste formelen, hvor $d = 2a$ er indre kardiameter, er *Hagen-Poiseuille's formel* for Newton-fluider.

5.6.3 STENOSER

Normal strømning av blod i arterier blir noen ganger forstyrret av innsnevninger av blodkaret. Disse kalles stenoser. En stenose representerer ofte en brå innsnevring over en kort lengde, se fig. 5.16, som viser en forenklet modell av en stenose. Fordi en stenose gjerne også impliserer avleiringer av fett og kalsium, vil karveggen få en lokal avstivning. Ved analyse av strømningen gjennom en stenose kan derfor deformasjon av karveggen neglisjeres. Under forutsetning om stasjonær, kan trykkfallet gjennom stenosene vist i fig. 5.16 beregnes til

$$\Delta P = P_1 - P_4 = \frac{8\pi\mu L Q}{A_s^2} + \frac{\rho Q^2}{2A^2} \left[\frac{A}{A_s} - 1 \right]^2 \quad (5.6.20)$$

Her er Q volumstrømmen, A arealet av kartverrsnittet og A_s arealet av det innsnevrede tverrsnittet, L er lengden av stenosene og μ er blodets viskositet. Det første leddet på høyre side i (5.6.20) er en såkalt *Borda-Carnot-effekt* som forårsakes av energitap i den turbulente strømningen i virvlene etter utløpet fra stenosene. Det andre leddet representerer friksjonstap mot karveggen i stenosene.

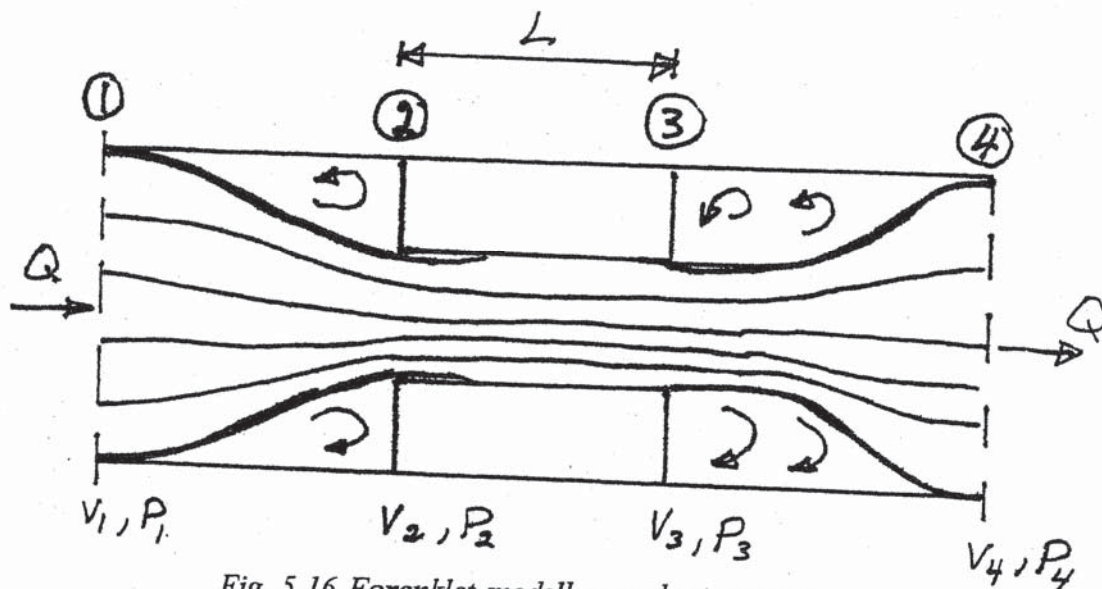


Fig. 5.16 Forenklet modell av en kort stenose.

Resultatet (5.6.20) vil nå bli utledet. I fig. 5.16 er vist fire stasjoner. Volumstrømmen Q er den samme gjennom stasjonene og for gjennomsnittshastighetene over tverrsnittene blir

$$v_1 = v_4 = \frac{Q}{A}, \quad v_2 = v_3 = \frac{Q}{A_s} \quad (5.6.21)$$

Vi kan dele strømningen gjennom stenosene opp i tre regioner. Mellom stasjon 1 og stasjon 2 bruker vi Bernoullis likning for rørstrømning, som når vi neglisjeres trykktap på grunn av viskositet og antar tilnærmet konstant hastighet over strømningstverrsnittene innenfor området markert med tykke strømlinjer i figuren, gir

$$\frac{v_1^2}{2} + \frac{P_1}{\rho} = \frac{v_2^2}{2} + \frac{P_2}{\rho} \quad (5.6.22)$$

Ved hjelp av relasjonene (5.6.21) ordnes likningen til

$$P_1 - P_2 = \frac{\rho Q^2}{2A^2} \left[\left(\frac{A}{A_s} \right)^2 - 1 \right] \quad (5.6.23)$$

Mellan stasjon 2 og stasjon 3 regner vi med et trykkfall basert på resultatet (5.6.19) for laminær rørstrømning av en Newton-fluid.

$$Q = \frac{\pi d^4}{128\mu} c \Rightarrow c = \frac{128Q\mu}{\pi d^4} = \frac{8\pi Q}{A_s^2} \quad (5.6.24)$$

Resultatet representerer en grov forenkling fordi strømningen i virkeligheten utvikles fra et tilnærmet uniformt (flat) hastighetsprofil ved innløpet ved stasjon 2 til et fullt utviklet parabolsk profil inne i stenosen. Fra likning (5.6.24) får vi

$$P_2 - P_3 = cL = \frac{8\pi\mu Q L}{A_s^2} \quad (5.6.25)$$

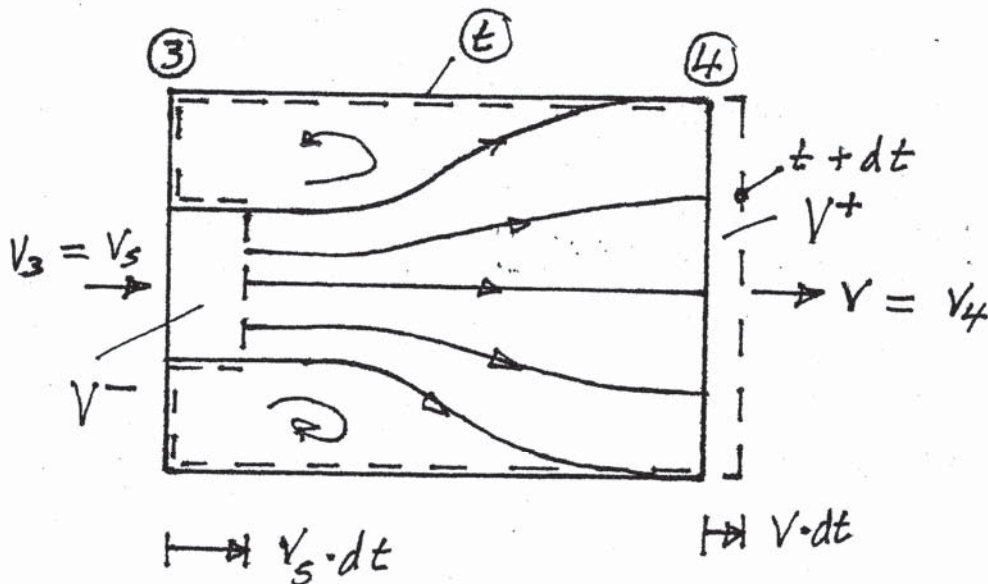


Fig. 5.17 Blodlegemet mellom stasjon 3 og stasjon 4 ved tidspunktene t og $t+dt$.

For å finne trykkfallet mellom stasjon 3 og stasjon 4 bruker vi kraftloven (Eulers 1. aksiom) for blodlegemet som ved tiden t befinner seg mellom de to stasjonene. Fig. 5.17 viser legemet ved tidspunktene t og $t+dt$. Fordi strømlinjene er rette og parallele både ved stasjon 3 og stasjon 4, er trykket konstant over strømingstverrsnittene ved disse stasjonene. Det viser seg også at trykket kan regnes konstant over hele tverrsnittet A ved stasjon 3. Det betyr at resulterende kraft i strømretningen på blodlegemet mellom stasjon 3 og stasjon 4 blir

$$f = P_3 \cdot A - P_4 \cdot A \quad (5.6.26)$$

Nå antar vi videre at hastigheten tilnærmet er uniform over strømingstverrsnittene ved begge stasjonene. Bevegelsesmengden for det volumet som er felles ved de to tidene er uendret. Men legemet får i løpet av tidsintervallet dt et tillegg i bevegelsesmengden fra volumet $V^+ = v \cdot dt \cdot A$ som blir lik $\rho(v \cdot dt \cdot A) \cdot v$. Dessuten mister legemet en bevegelsesmengde fra volumet $V^- = v_s \cdot dt \cdot A_s$, og dette fradraget blir lik $\rho(v_s \cdot dt \cdot A_s) \cdot v_s$. Endring av legemets bevegelsesmengde per tidsenhet blir derfor

$$\dot{p} = \rho v A v - \rho v_s A_s v_s = \rho \frac{Q^2}{A} \left[1 - \frac{A}{A_s} \right] \quad (5.6.27)$$

Dermed gir kraftloven

$$f = \dot{p} \Rightarrow P_3 A - P_4 A = \rho \frac{Q^2}{A} \left[1 - \frac{A}{A_s} \right] \Rightarrow$$

$$P_3 - P_4 = \rho \frac{Q^2}{A^2} \left[1 - \frac{A}{A_s} \right] \quad (5.6.28)$$

Addisjon av de tre likningene (5.6.23, 25, 28) gir nå resultatet (5.6.20)

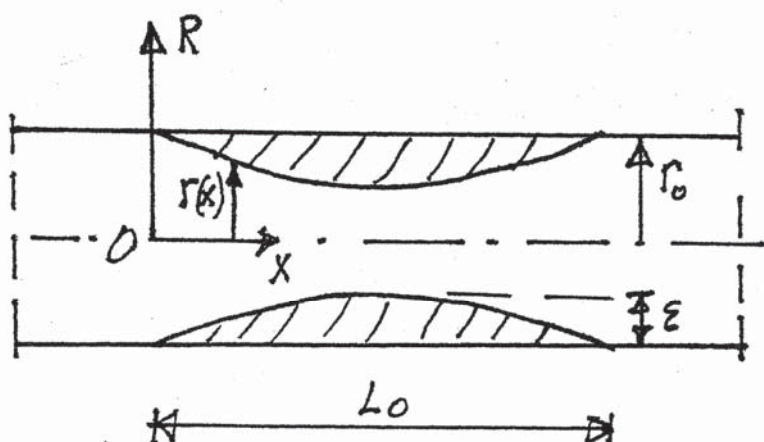


Fig. 5.18 Stenosegeometri etter Haldar og Dey [2].

Et eksempel på beregning av sammenhengen mellom trykkgradienten gjennom en stenose og volumstrømmen er gitt i en artikkel av Haldar og Dey [Arch. Mech., vol. 42, I, pp 109-114, Warszawa 1990]. Fig. 5.18 viser geometrien som antas. Innsnevringen er gitt ved

$$\frac{r(x)}{r_0} = 1 - \frac{\varepsilon}{2r_0} \left[1 + \cos \frac{2\pi}{L_0} \left(x - \frac{L_0}{2} \right) \right] \quad \text{for } 0 \leq x \leq L_0 \quad (5.6.29)$$

Som viskositetsfunksjon foreslås

$$\eta(H) = \frac{\mu_0}{1 - \beta H} \quad (5.6.30)$$

hvor μ_0 er viskositeten til blodplasma, β er en konstant satt lik 2,5 og H er hematocrit. Det er videre antatt at H varierer med avstanden R fra karaksen etter formelen

$$H(R) = H_m \left[1 - \left(\frac{R}{r_0} \right)^n \right] \quad (5.6.31)$$

Denne formelen tar hensyn til at de røde blodlegemene har størst konsentrasjon nær karaksen. H_m og n er konstante parametere.

Trykkgradienten $\partial P / \partial z$ varierer gjennom stenosen med koordinaten z . Ved å følge fremgangsmåten demonstrert i seksjon 5.5.4, kan vi nå utvikle følgende resultater for hastighetsfeltet $v(R)$ og for trykkgradienten

$$v(R) = \frac{r_0^2}{4\mu} \frac{\partial P}{\partial x} \left\{ (1-k) \left[\left(\frac{r}{r_0} \right)^2 - \left(\frac{R}{r_0} \right)^2 \right] + \right. \\ \left. + \frac{2k}{n+2} \left[\left(\frac{r}{r_0} \right)^{n+2} - \left(\frac{R}{r_0} \right)^{n+2} \right] \right\} \quad (5.6.32)$$

$$\left| \frac{\partial P}{\partial x} \right| = \frac{8\mu Q}{\pi r_0^4} \frac{1}{(1-k) \left(\frac{r}{r_0} \right)^4 + \frac{4k}{n+4} \left(\frac{r}{r_0} \right)^{n+4}} \quad (6.2.16)$$

Q er volumstrømmen og $k = \beta H_m$. Setter vi $r = r_o$, får vi trykkfallet i blodkaret utenfor stenosen

$$\left| \frac{dP}{dx} \right|_0 = \frac{8\mu Q}{\pi R_0^4} \frac{1}{1 - \frac{kn}{n+4}} \quad (5.6.34)$$

Fig. 5.19 viser forlopet av trykkgradienten gjennom stenosen. Setter vi $\beta = 0$ i funksjonen (5.6.30), har vi en Newton-fluid. Da blir $k = 0$, og formel (6.2.17) gir Hagen-Poiseuille's formel (5.6.19).

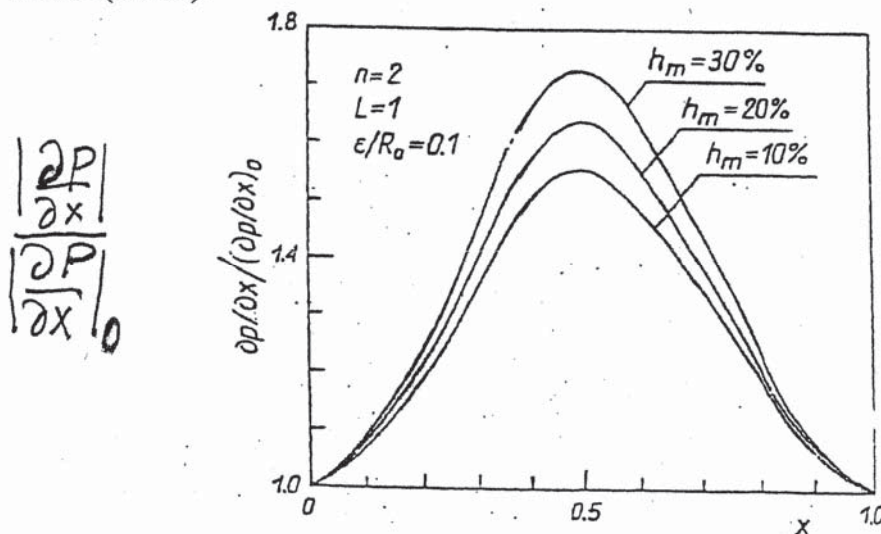


Fig. 5.19 Trykkgradienten som funksjon av avstand x gjennom stenosen.

5.7 BØLGER I ELASTISKE BLODKAR

I denne seksjonen skal vi diskutere den pulsatile blodstrømningen i elastiske blodkar. Vi starter med å betrakte blodkaret som et langt rett elastisk rør hvor igjennom det strømmer blod på grunn av en et pulsatilt modifisert trykk $P(x, t)$. x er koordinaten langs karaksen. Fig. 5.20 viser en seksjon dx av et elastisk blodkar fylt med blod. Arealet av kartverrsnittet er $A(x, t)$. Vi antar uniformt hastighetsprofil $v(x, t)$ over tverrsnittet, slik at volumstrømmen kan uttrykkes ved $Q = Av$. I løpet av et kort tidsintervall dt endrer karet form. Blodlegemet som var i karet ved tidspunktet t , er ved tidspunktet $t + dt$ markert ved den strekmerkede konturen. Blod regnes som en inkompresibbel fluid og volumet må være det samme til alle tider. Forskjellen på volumene til legemene ved de to tidspunktene må være lik null. Derfor blir

$$-V_1 + V_2 + V_3 = 0 \Rightarrow -Av \cdot dt + \left[\frac{\partial A}{\partial t} dt dx \right] + \left[Av + \frac{\partial Av}{\partial x} dx \right] = 0 \Rightarrow$$

$$\frac{\partial A}{\partial t} + \frac{\partial (Av)}{\partial x} = 0 \quad (5.7.1)$$

som er kontinuitetslikningen for dette tilfellet. Kraftloven (Eulers 1. aksiom) for det samme blodlegemet skal nå brukes for å få frem en dynamisk likning. Legemet er påvirket av trykk på overflaten og skjærspenning τ på flaten mot karveggen. Resultanten av trykket P mot flaten mot karveggen kan settes lik $P(\partial A/\partial x)dx$. Resulterende kraft i strømningsretningen blir derfor

$$df = PA + P \frac{\partial A}{\partial x} dx + \tau \pi D dx - \left[PA + \frac{\partial (PA)}{\partial x} dx \right] \Rightarrow$$

$$df = \left[-A \frac{\partial P}{\partial x} + \pi D \tau \right] dx \quad (5.7.2)$$

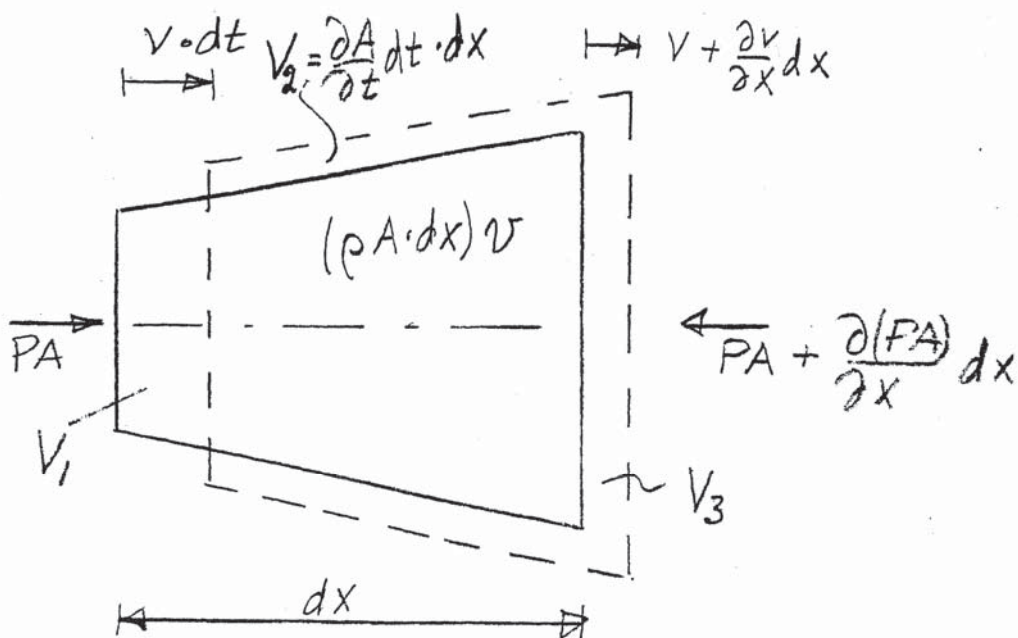


Fig. 5.20 Seksjon av blodkar fylt med blod.

Endring av bevegelsesmengden for det volumet som er felles ved de to tidspunktene kalles dp_f . Volumet V_1 representerer et fradrag dp_1 , mens volumene V_2 og V_3 gir et tillegg i bevegelsesmengde når legemet beveger seg i tidsintervallet dt . Ut fra antagelsen om uniform hastighet over kartverrsnittet blir

$$\begin{aligned} dp_f &= \frac{\partial}{\partial t}[(\rho A dx) v] dt, \quad dp_1 = -(\rho A v dt) v \\ dp_3 &= (\rho A v dt) v + \frac{\partial}{\partial x}[(\rho A v dt) v] dx, \quad dp_2 = \left[\frac{\partial A}{\partial t} dt dx \right] v \frac{1}{dt} \end{aligned} \quad (5.7.3)$$

Per tidsenhet blir endring i bevegelsesmengde for blodlegemet

$$\dot{dp} = \left[\rho \frac{\partial A v}{\partial t} + \rho \frac{\partial(A v^2)}{\partial x} \right] dx = \rho A \left[\frac{\partial v}{\partial t} + v \frac{\partial v}{\partial x} \right] \quad (5.7.4)$$

Dermed gir kraftloven

$$\begin{aligned} df = \dot{dp} &\Rightarrow \left[-A \frac{\partial P}{\partial x} + \pi D \tau \right] dx = \rho A \left[\frac{\partial v}{\partial t} + v \frac{\partial v}{\partial x} \right] dx \Rightarrow \\ \frac{\partial v}{\partial t} + v \frac{\partial v}{\partial x} &= -\frac{1}{\rho} \frac{\partial P}{\partial x} + \frac{\pi D}{\rho} \tau \end{aligned} \quad (5.7.5)$$

Vi antar nå at skjærspenningen τ kan neglisjeres. Det vil si at vi regner blod som en perfekt fluid. Vi skal kommentere denne antagelsen senere. Dermed reduseres bevegelseslikningen (5.7.5) til

$$\frac{\partial v}{\partial t} + v \frac{\partial v}{\partial x} = -\frac{1}{\rho} \frac{\partial P}{\partial x} \quad (5.7.6)$$

Vi har nå to likninger som styrer strømningen i blodkaret: kontinuitetslikning (5.7.1) og bevegelseslikningen (5.7.6).

La v_o , A_o , $P_o(x)$ og Q_o være henholdsvis hastighet, tverrsnittsareal, trykk og volumstrøm til en stasjonær blodstrømning gjennom blodkaret. Et pulserende trykk og det resulterende hastighetsfeltet uttrykkes slik

$$P_o + P(x,t) , v_o + v(x,t) \quad (5.7.9)$$

Dette resulterer i et tverrsnittsareal og en volumstrøm gitt henholdsvis ved

$$A_o + A(x,t) , Q_o + Q(x,t) \quad (5.7.10)$$

Vi antar at tilleggsfunksjonene: v , A , P og Q er små størrelser sammen med respektive stasjonære funksjoner: v_o , A_o , P_o og Q_o . Det fører til at likningene (5.7.1) og (5.7.6) reduseres til henholdsvis

$$\frac{\partial A}{\partial t} + A_o \frac{\partial v}{\partial x} + v_o \frac{\partial A}{\partial x} = 0 \quad (5.7.11)$$

$$\frac{\partial v}{\partial t} + v_o \frac{\partial v}{\partial x} = - \frac{1}{\rho} \frac{\partial P}{\partial x} \quad (5.7.12)$$

Vi innfører her et nytt koordinatsystem som beveger seg med den stasjonære strømningen. Det gjøres ved å erstatte koordinatene (x, t) med koordinatene (X, T) , slik at

$$X = x - v_o t , T = t \quad (5.7.13)$$

Vi finner nå

$$\frac{\partial}{\partial t} = \frac{\partial}{\partial T} \frac{\partial T}{\partial t} + \frac{\partial}{\partial X} \frac{\partial X}{\partial t} = \frac{\partial}{\partial T} - v_o \frac{\partial}{\partial X} , \frac{\partial}{\partial x} = \frac{\partial}{\partial T} \frac{\partial T}{\partial x} + \frac{\partial}{\partial X} \frac{\partial X}{\partial x} = \frac{\partial}{\partial X}$$

og får

$$\frac{\partial v}{\partial t} + v_o \frac{\partial v}{\partial x} = \frac{\partial v}{\partial T} - v_o \frac{\partial v}{\partial X} + v_o \frac{\partial v}{\partial X} = \frac{\partial v}{\partial T}$$

slik at bevegelseslikningen (5.7.6) reduseres til

$$\frac{\partial v}{\partial T} = - \frac{1}{\rho} \frac{\partial P}{\partial X} \quad (5.7.14)$$

Kontinuitetslikningen (5.7.11) omformes slik

$$\frac{\partial A}{\partial t} + A_o \frac{\partial v}{\partial x} + v_o \frac{\partial A}{\partial x} = \frac{\partial A}{\partial T} - v_o \frac{\partial A}{\partial X} + A_o \frac{\partial v}{\partial X} + v_o \frac{\partial A}{\partial X} = 0 \Rightarrow$$

$$\frac{\partial A}{\partial T} + A_o \frac{\partial v}{\partial X} = 0 \quad (5.7.15)$$

Vi trenger nå en konstitutive likning for blodkaret, og vi antar en lineær sammenheng mellom trykket P og tverrsnittsarealet A .

$$A(P) = A_o + K(P - P_o) \quad (5.7.16)$$

Koeffisienten K kalles *kompliansen*.

$$K = \frac{\partial A}{\partial P} \quad (5.7.17)$$

Nå blir

$$\frac{\partial A}{\partial T} = \frac{\partial A}{\partial P} \frac{\partial P}{\partial T} = K \frac{\partial P}{\partial T} \quad (5.7.18)$$

Dette settes inn i kontinuitetslikningen (5.7.15) og gir

$$K \frac{\partial P}{\partial T} + A_o \frac{\partial v}{\partial X} = 0 \quad (5.7.19)$$

Ved å partiell-derivere likning (5.7.14) med hensyn til T og likning (5.7.19) med hensyn til X og så subtrahere likningene fra hverandre, får vi den endimensjonale bølgelikningen for hastigheten $v(X, T)$

$$\frac{\partial^2 v}{\partial T^2} = c^2 \frac{\partial^2 v}{\partial X^2}, \quad c = \sqrt{\frac{A_o}{\rho K}} \quad (5.7.20)$$

Ved å partiell-derivere likning (5.7.19) med hensyn til T og likning (5.7.14) med hensyn til X og så subtrahere likningene fra hverandre, får vi den endimensjonale bølgelikningen for trykket $P(X, T)$

$$\frac{\partial^2 P}{\partial T^2} = c^2 \frac{\partial^2 P}{\partial X^2}, \quad c = \sqrt{\frac{A_o}{\rho K}} \quad (5.7.21)$$

Chapter 6

MUSCLES

6.1 INTRODUCTION

There are three kinds of muscles in the body: skeletal muscles, heart muscles, and smooth muscles. Skeletal muscles make up a major part of the animal body. While the skeletal muscle and the heart muscle are controlled by voluntary nerves, that is not the case with the smooth muscles. The following presentation is extracted from Fung's book [1].

6.2 THE SKELETAL MUSCLE

Figure 6.1 shows the organizational hierarchy of a skeletal muscle. The unit of the skeletal muscle is the *muscle fiber*, which is a single cell provided with many nuclei. The fibers are arranged in *bundles*, called *fasciculi*, of various sizes within the muscle. Connective tissue fills the spaces between the muscle fibers within a bundle. Each bundle is surrounded by a strong connective tissue sheath (mantel), and the whole muscle is again surrounded by an even stronger sheath.

The length of a muscle fiber may vary from some mm to several cm. Sometimes the length can reach 30 cm in long muscles. The diameter of the fiber is 10-60 μm . A fiber may stretch from one end of the muscle to the other length, but often extends only part of the length of muscle, ending in tendinous or other connective tissue intersection.

Each muscle fiber consists of many longitudinal threads called myofibrils. Each myofibril is composed of arrays of myofilaments, see Figure 6.2, which again are divided into serially repeated regions termed sarcomeres, each about 2 μm long. The sarcomere is the active part of the myofilament. The sarcomere is made of two types of filaments: the actin filament and the myosin filament. The contractile action of the muscle is due to an interaction of these two types of filaments.

If the skeletal muscle is stimulated at a sufficiently high frequency, it generates a maximum tension, which remains constant in time. The muscle is said to be tetanized. The activity of the contracting mechanism is then thought to be maximal. The stress of the skeletal muscle may be negligible. For instance a frog muscle can deliver a maximum stress of 200 kPa at its optimal length.

Skeletal muscles respond to stimulation by nervous, electrical or chemical impulses. Each adequate stimulation gives a single twitch lasting for a fraction of a second. successive

twitches may add up to produce a stronger action. The successive contractions fuse together and cannot be distinguished from each other. This leads to what is called a tetanized state in the muscle. Figure 6.2 indicate the wave summation of twitches.

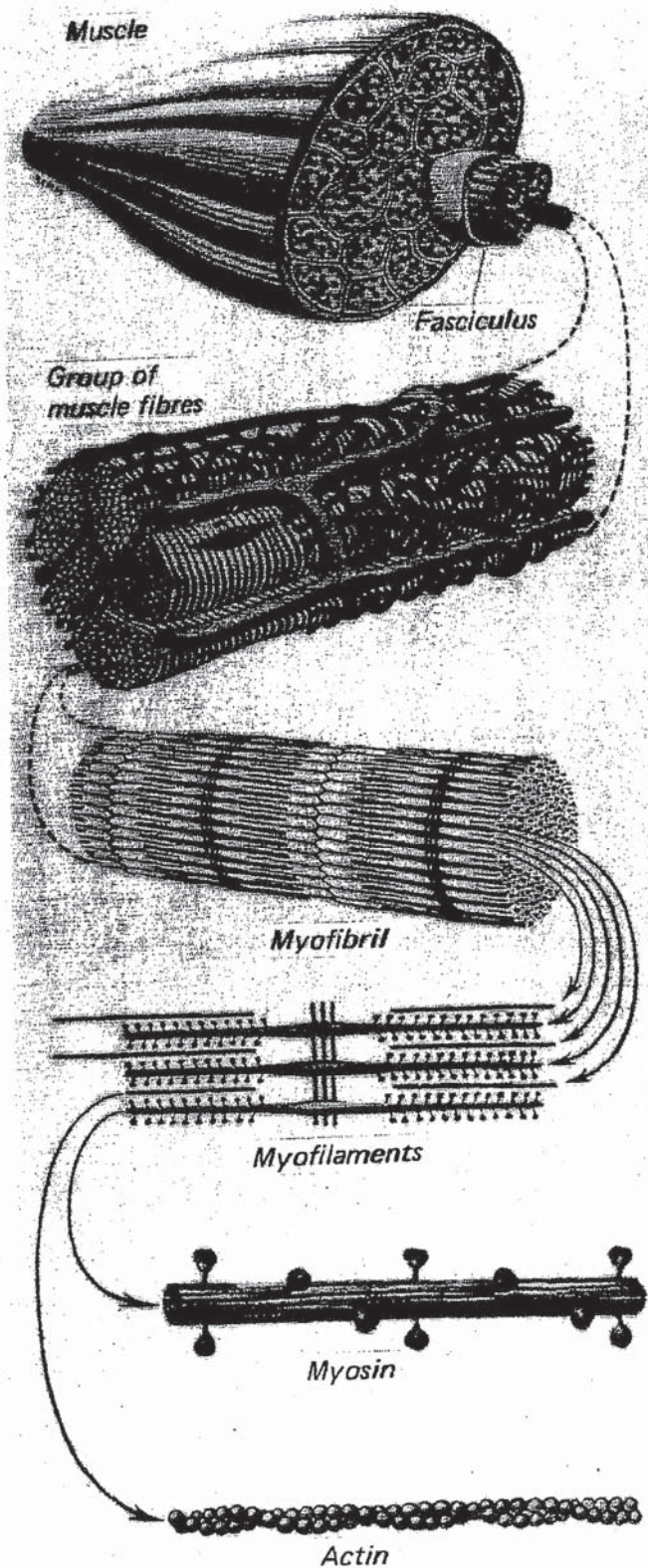


Fig. 6.1 The organizational hierarchy of a skeletal muscle. From Fig. 9.3.1 in Fung [1].

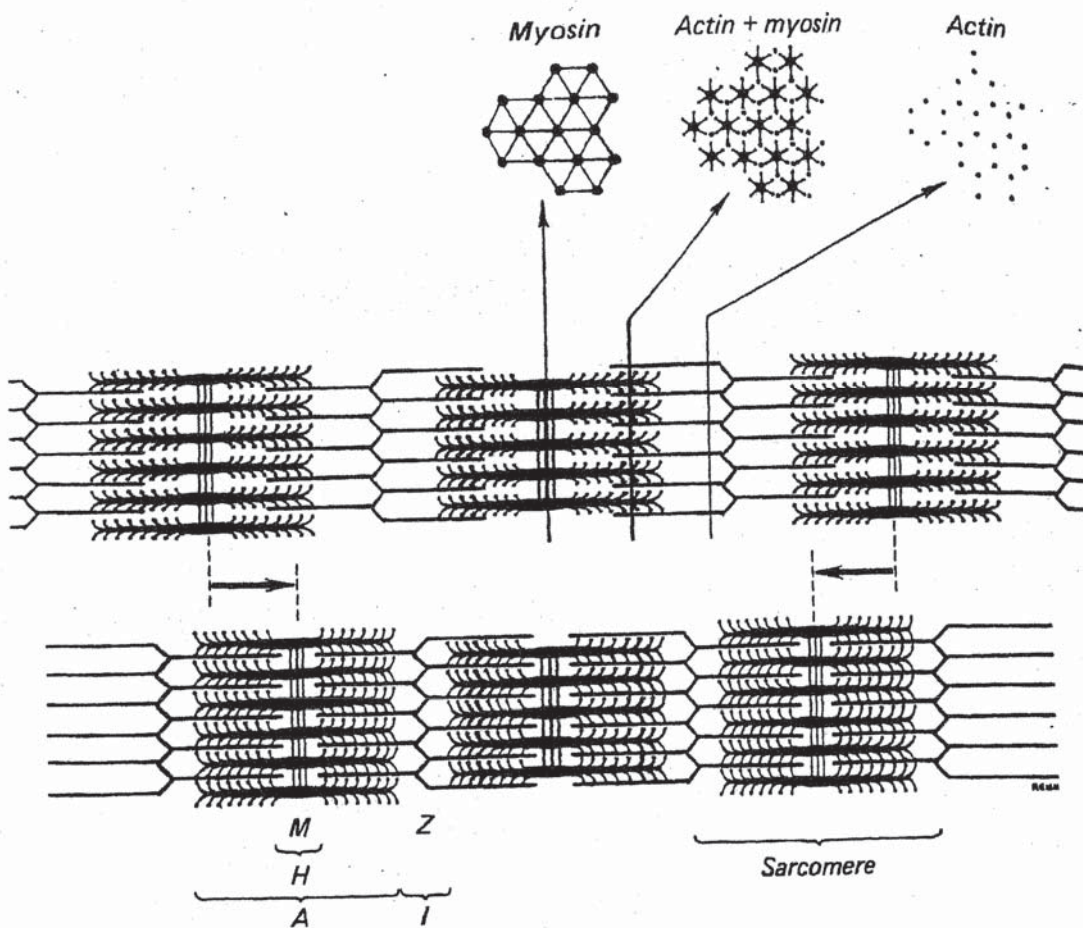


Fig. 6.2 The structure of a myofilament. From Fig. 9.3.2 in Fung [1].

6.2.1 HILL'S EQUATION

Figure 6.3 shows a muscle in a tetanized condition after electrical stimulation. The muscle force is a function of the length L_o : $T_o(L_o)$. The muscle is now released to a force $T < T_o$. Contraction of the muscle starts and the velocity of shortening $v = - dL/dt$ is measured. Experiments then confirm the relationship (6.1.1), called the Hill's equation.

$$(v + b)(T + a) = b(T_o + a) \quad (6.2.1)$$

a and b are constant parameters. The equation may be rewritten to give

$$\frac{T}{T_o} = \frac{1 - v/v_o}{1 + c(v/v_o)} , \quad \frac{v}{v_o} = \frac{1 - (T/T_o)}{1 + c(T/T_o)} , \quad v_o = \frac{bT_o}{a} , \quad c = \frac{T_o}{a} \quad (6.2.2)$$

The maximum isometric tension T_o depends strongly on the sarcomere length L_o . Figure 6.4 shows this relationship for a single fiber of a frog's skeletal muscle. The velocity parameter v_o does depend slightly on the length L_o while the parameter c seems almost independent of L_o .

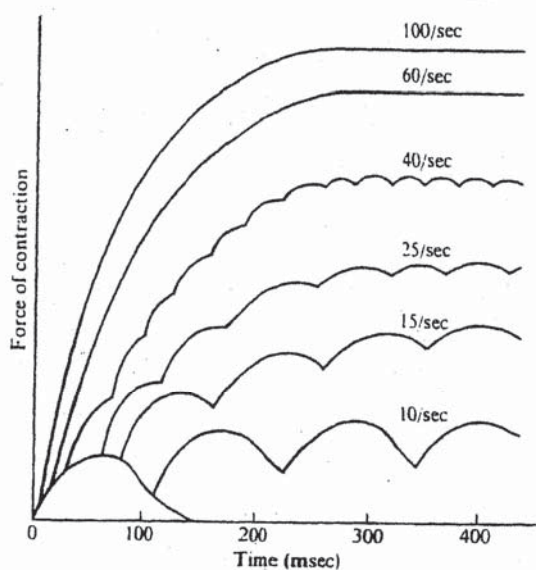


Fig. 6.3 Wave summation and tetanization. From Fig. 9.5.1 in Fung [1].

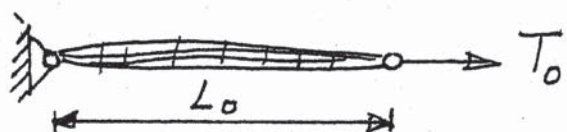


Fig. 6.4 Muscle in a tetanized condition after electrical stimulation.

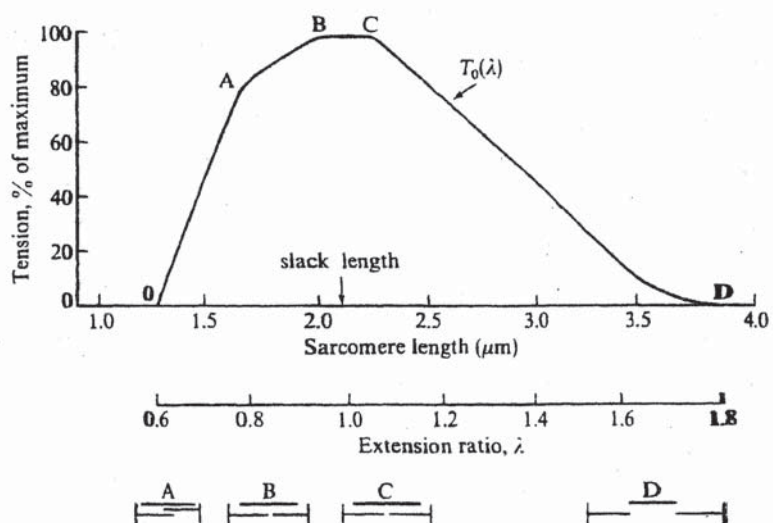


Fig. 6.5 The isometric tension-stretch curve $T_0(\lambda)$. From Fig. 9.7.2 in Fung [1].

6.2.2 HILL'S THREE-ELEMENT MODEL

Hill's equation was derived from quick-release experiments on a frog muscle in tetanized condition. It cannot describe a single twitch or the force-velocity relationship when tetanized muscle is subjected to a slow release, nor to a strain that varies with time. Hill has proposed a three-element mechanical model, shown in Figure 6.4a, to simulate the general behavior of a muscle. The model carries a force T and consists of two elements in series: a contractile element CE responsible for the active response of the muscle and a elastic spring element SE , and a parallel elastic spring element PE . The elements in series carries the load S and the parallel element carries the load P . Figure 6.6b shows the physiological model of the muscle sarcomere. Sections 9.8.1-4, pages 405-411 in Fung's book describe how Hill's three parameter model works and present two experiments which are used to determining the characteristics of the series elastic element.

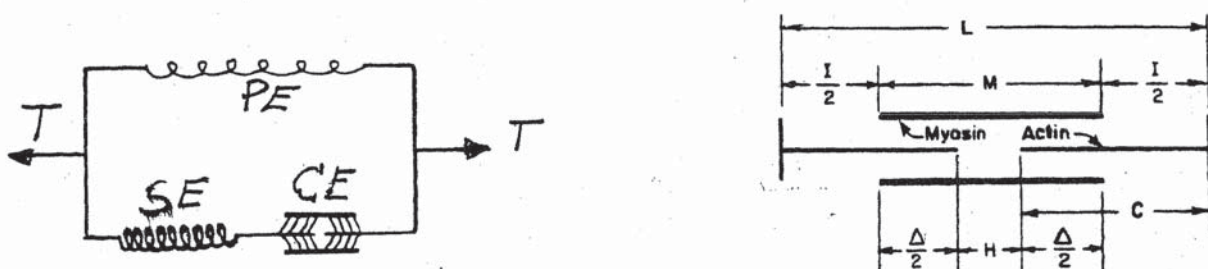


Fig. 6.6 a) Hill's three-element mechanical model of a muscle. b) the physiological muscle model of a muscle fiber, from Fig. 9.8.2 in Fung [1].

6.3 THE HEART MUSCLE

The heart muscle, or the myocardial muscle, is never tetanized in its normal function. The muscle functions in single twitches. Each electric stimulation evokes one twitch, which has to run its course. The resting heart muscle is stiffer than the resting skeletal muscle, and the resting stress is not negligible as it is for a skeletal muscle. The basic mechanism of contraction are similar, but important differences exist.

6.3.1 THE UNSTIMULATED HEART MUSCLE

The Hill's three-element mechanical model is extended to a four-element model as shown in Figure 6.7. The parallel branch is subdivided to include an elastic spring and a dashpot (damper). The unstimulated muscle now behaves as a viscoelastic material, see Section 1.5. When the muscle is unstimulated the force S in the contractile branch is zero. The force carried by the muscle is then $T = P$. In a stress relaxation test the muscle is subjected to a constant strain ε , here represented by a constant stretch $\lambda = 1+\varepsilon$. If the initial force is P , the test records the *relaxation function* $G(t)$.

$$G(t) = \frac{P(t)}{P_r} \quad , \quad P(t) = P(\lambda, \theta, t) \quad (6.3.1)$$

where θ is the temperature. Figure 6.8 shows how the relaxation function depends on the stretch and the temperature for a rabbit papillary muscle, which is a muscle controlling a valve, the mitral valve, inside the left ventricle of the heart.

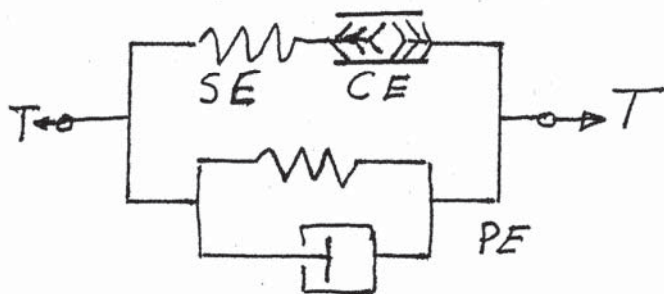


Fig. 6.7 A four-element mechanical model.

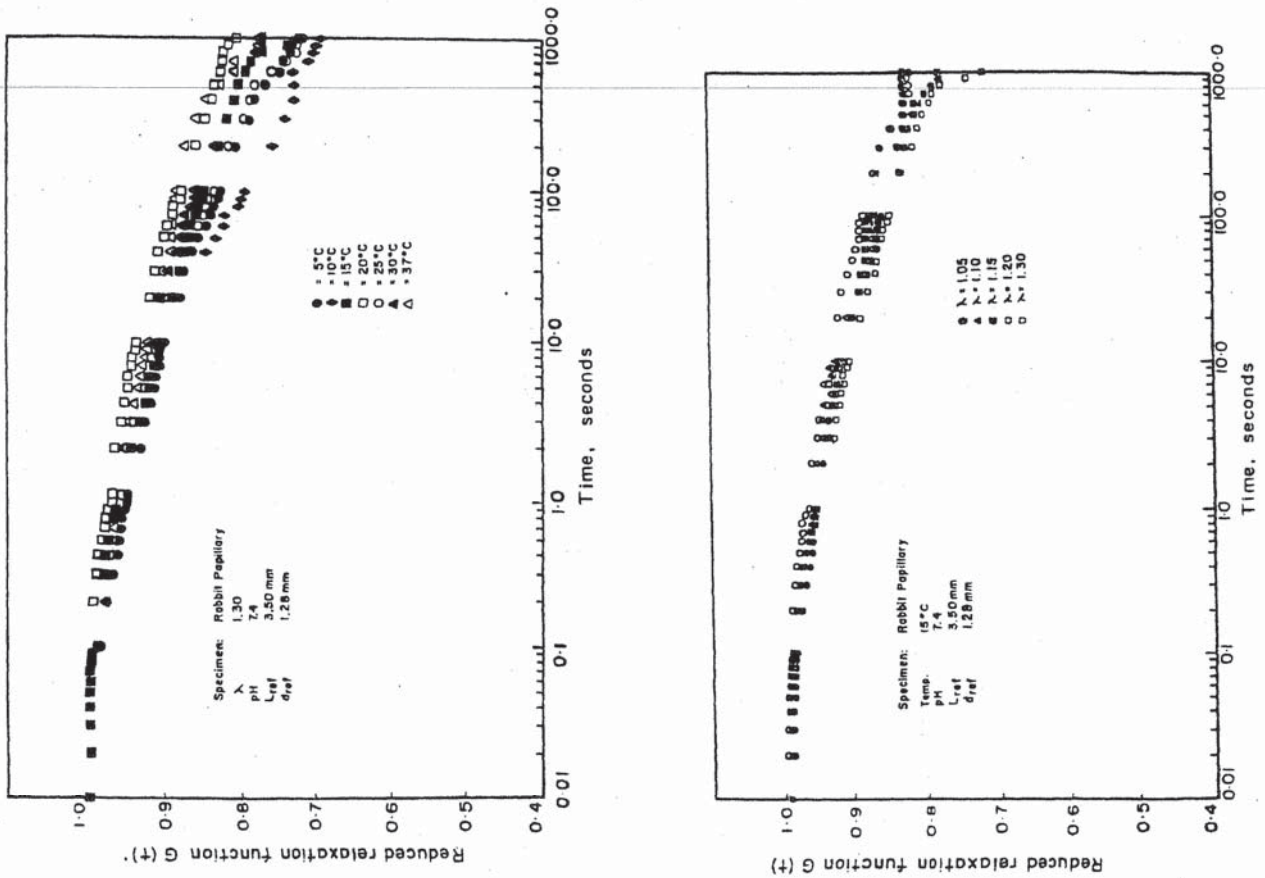


Fig. 6.8 Relaxation function of a rabbit papillary muscle. From Fig. 10.4.1-2 in Fung [1].

The experimental results shown in Figure 6.8 suggest that the force may be expressed by

$$P(\lambda, \theta, t) = G(t) P^e(\lambda, \theta) \quad (6.3.2)$$

where the relaxation function $G(t)$ is a function of time only and so defined that $G(0) = 0$. The function $P^e(\lambda, \theta)$ is called the elastic response. A general stretch history $\lambda(t)$ may be considered as a sum of stretch increments, each of which represents a relaxation test. Superposition of stress contributions from all increments may then be used to obtain the total stress. This process leads to $P^e(\lambda, \theta, t)$ being expressed by a convolution integral.

The elastic response $P^e(\lambda, \theta)$ cannot be measured directly from experiments. But when $G(t)$ has been determined, equation (6.3.2) may be used to get $P^e(\lambda, \theta)$ indirectly. Figure 6.9 shows the elastic response of the rabbit papillary muscle. Note that the response is different in loading and unloading. The following relationship may be extracted from Figure 6.6 in the case of uniaxial loading.

$$\frac{dP^e}{d\lambda} = \alpha(P^e + \beta) \Rightarrow P^e(\lambda) = [P^e(\lambda_o) + \beta] e^{\alpha(\lambda - \lambda_o)} - \beta \quad (6.3.3)$$

where λ_o is a reference value.

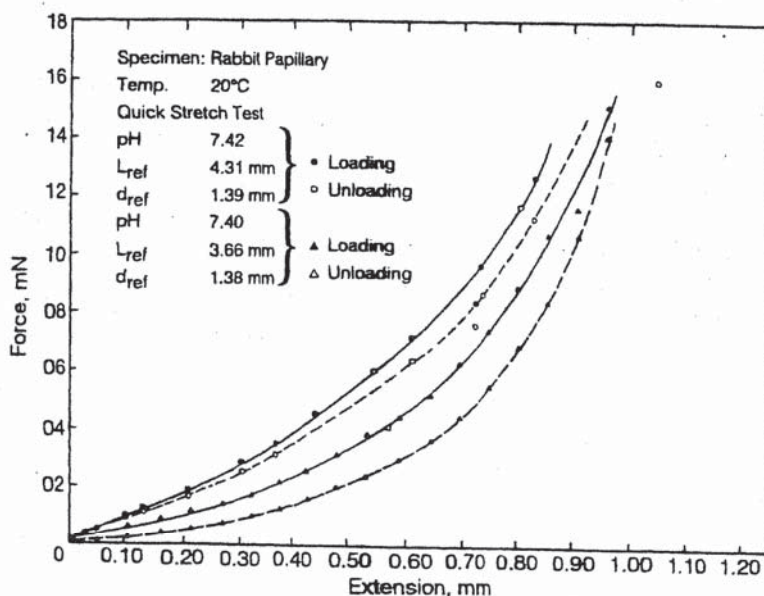


Fig. 6.9 Elastic response $P^e(\lambda, \theta)$ of a rabbit papillary muscle. From Fig. 10.4.3 in Fung [1].

6.3.2 THE ACTIVE MYOCARDIUM. STIMULATED HEART MUSCLE

Several attempts have been made to establish a constitutive relation for the force S in the contractile branch in the Hill's three-parameter model, Figure 6.6a. In 1987 Pinto proposed the following expression for the force S .

$$S(\lambda, t) = A(\lambda)t^\nu e^{-\delta t} \quad (6.3.4)$$

The stretch λ is measured relative to a reference state at which the S is zero. The parameter ν is introduced to account for contraction delay. The parameter δ is introduced to account for the contractile state of the muscle at a given physiological condition. The total force in the muscle is now

$$T(\lambda, t) = P(\lambda, t) + A(\lambda)t^\nu e^{-\delta t} \quad (6.3.5)$$

Pinto and Boe (1991) proposed a special method to find the passive stress function $P(\lambda, t)$.

The test specimen used in evaluating the active and the passive stress functions is often the papillary muscle in the left ventricle that controls the mitral valve for blood entering the left ventricle from the atrium.

Chapter 7

HEART MODELS

7.1 INTRODUCTION

Figure 7.1 presents a sketch of the anatomy of the human heart. The blood used in the body is transported through veins to the right atrium *RA*, and flows through the tricuspid valve *TV* into the right ventricle *RV*, from where it is pumped through the pulmonary valve *P* and flows into the lungs through the pulmonary arteries *PA*. From the lungs the blood is transported through the pulmonary veins to the left atrium *LA*, and then flows through the mitral valve *M* into the left ventricle *LV*. The left ventricle is the high pressure heart pump that supplies the body with blood through the aortic valve *Ao* to the aorta and further to the arteries in the body. The pumping cycle of the heart consists of contraction, the *systole*, during which the pressure is created, and the dilatation or the filling of blood in the *LV*, the *diasstole*.

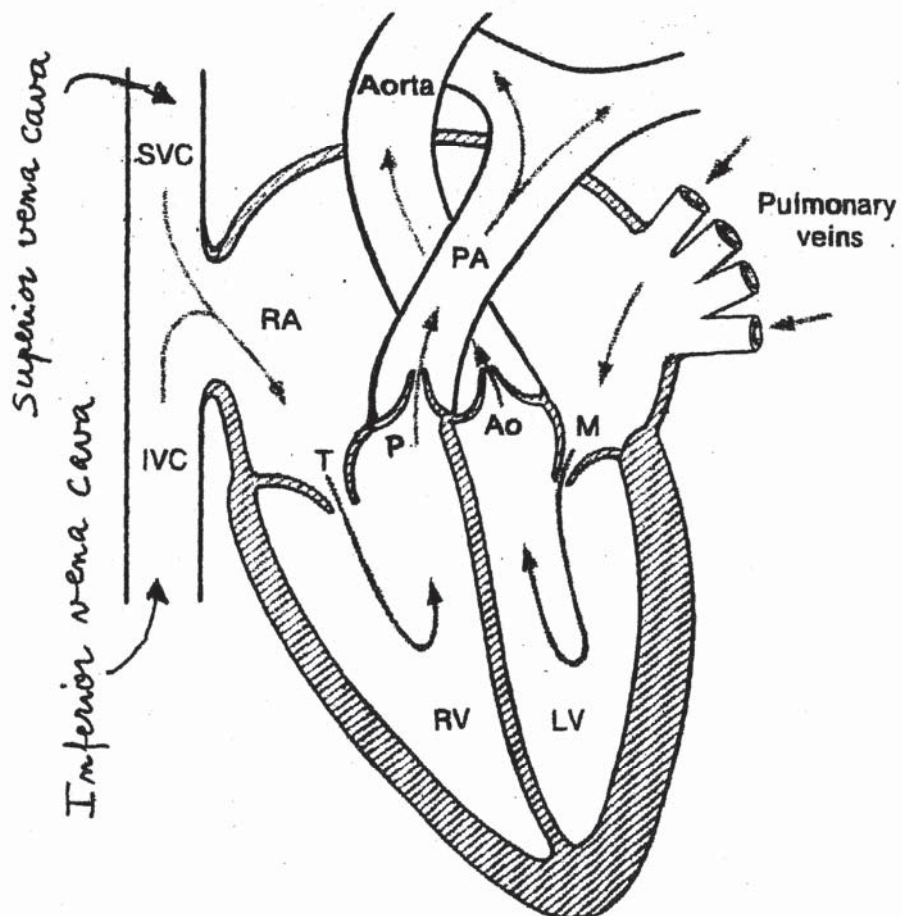


Fig. 7.1 The human heart

7.2 SIMPLIFIED MODELS OF THE LEFT VENTRICLE

In clinical research left ventricular wall stress and fiber shortening or fiber strain have been used to analyze myocardial oxygen consumption, the *LV* systolic function, and the *hypertrophy* caused by pressure and volume overload. The term *hypertrophy* means excessive growth or development of an organ or tissue.

Direct measurements of the wall stress with force/pressure transducer inserted into the wall are difficult because the transducer damages the tissue at the site of measurements. Wall stress has thus been estimated by using measurements of *LV* blood pressure and the geometry in mathematical models of the mechanics of the myocardium (= heart muscle).

The muscle fibers in the *LV* wall are approximately parallel to the wall, but the orientation changes through the thickness of the wall. Figure 7.2a presents a symmetric model of the *LV*. The figure indicates the fiber orientations. The angle of inclination with respect to the plane perpendicular to the long axis of the *LV* is denoted α . Figure 7.2b shows two approximate graphs of the angle as a function of the distance w from the middle surface of the wall. The change in α is greatest near the endocardial surface (= inner surface) and near the epicardial surface (= outer surface). This gives an *S-shaped* function $\alpha(w)$ for the fiber orientation distribution through the wall, with the middle surface fibers going mainly circumferential. Some studies present wall $\alpha(w)$ as a linear function, as indicated in Figure 7.2b.

Theoretical studies of Arts et al. [1] showed that when the base of the *LV* is free to rotate, the calculated fiber stress is nearly homogeneous. This allows for significant simplification in the modelling of the mechanisms of the *LV*.

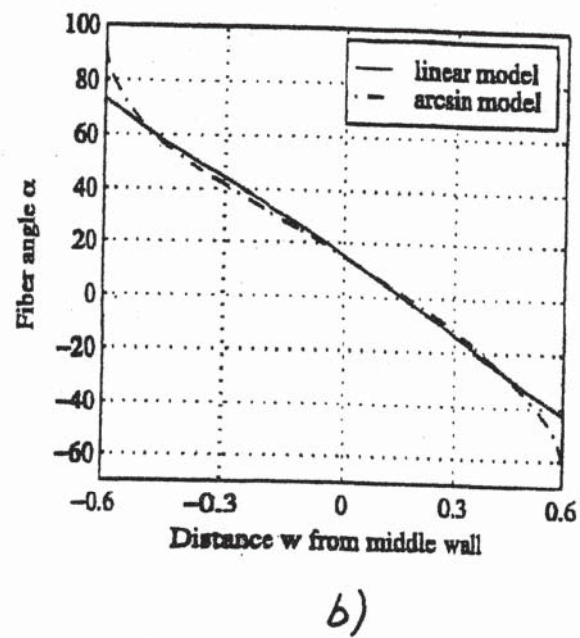
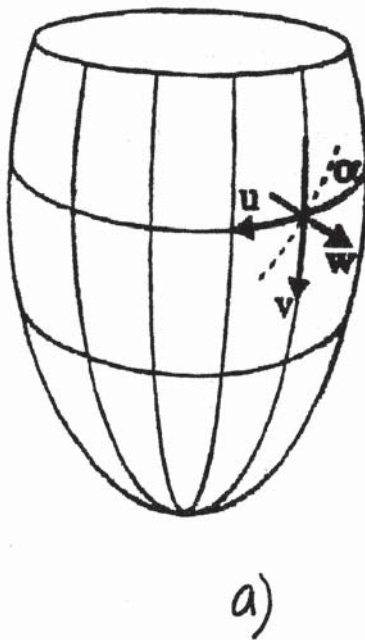


Fig. 7.2 a) Symmetric model of *LV*. b) Fiber angle as a function of thickness parameter w .

7.2.1 THE FLUID-FIBER CONTINUUM

Chadwick [2] proposed a mechanical model of the *LV* in which he regarded the myocardium as a fluid-fiber continuum. The myocardium is considered to be a soft incompressible material embedding muscle fibers, which only support forces in their longitudinal direction. The fluid-fiber continuum is thus a model of the active myocardium where the muscle fiber stress is much higher than the stresses in the connective tissue. The constitutive equation of the fluid-fiber continuum gives the stress tensor T in terms of an isotropic pressure p , the fiber stress σ , and the fiber direction, represented by a unit vector n . It may be shown that the proper representation of this constitutive equation is

$$T_{ij} = -p\delta_{ij} + \sigma n_i n_j \quad (7.2.1)$$

This result may be obtained from the Cauchy stress theorem (2.3.21). The fiber stress σ may be modelled as discussed in Section 6.2. In Figure 7.3 the fiber direction is defined by $n = [\cos\alpha, \sin\alpha, 0]$ and equation (7.2.1) yields

$$\begin{aligned} T_{11} &= -p + \sigma \cos^2\alpha, & T_{22} &= -p + \sigma \sin^2\alpha \\ T_{12} &= \sigma \sin\alpha \cos\alpha, & T_{33} &= -p \end{aligned} \quad (7.2.2)$$

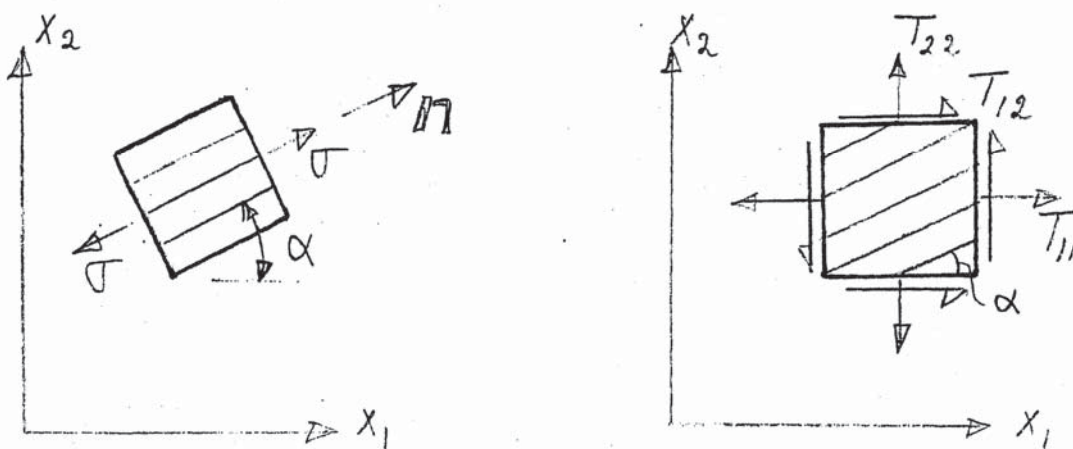


Fig. 7.3 Fluid-fiber continuum.

7.2.2 THE ARTS MODEL OF THE LEFT VENTRICLE

Arts et al. [1] present a simplified model of *LV* as a thick-walled cylinder, Figure 7.4. If it may be assumed that the muscle fibers lie in concentric cylindrical layers then from equation (7.2.2) the stresses on the coordinate planes of cylindrical coordinates (R, θ, z) become

$$\begin{aligned} \sigma_R &= -p, & \sigma_\theta &= -p + \sigma \cos^2\alpha, & \sigma_z &= -p + \sigma \sin^2\alpha \\ \tau_{\theta z} &= \sigma \sin\alpha \cos\alpha \end{aligned} \quad (7.2.3)$$

where α is the angle between the muscle fiber and the plane perpendicular to the axis of the cylinder.

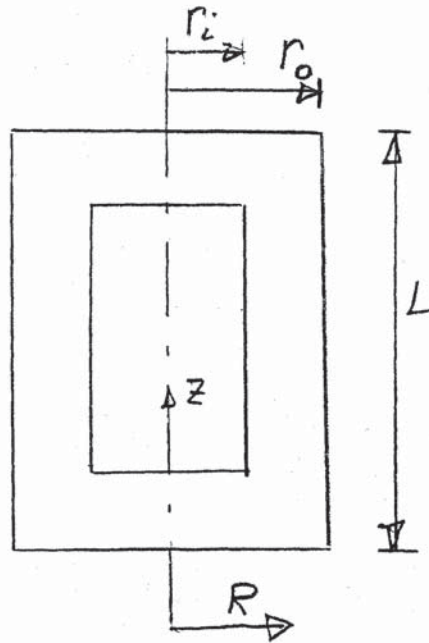
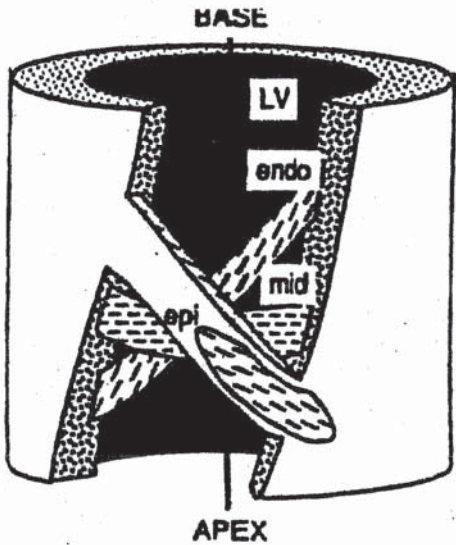


Fig. 7.4 The Arts model of the left ventricle.

The thick-walled cylinder is considered to consist of many thin-walled shells of thickness dR , Figure 7.5. Figure 7.5a shows an element of height dz of a thin shell. Equilibrium of the element implies

$$dp \cdot (2R \cdot dz) + (\sigma_\theta + p) \cdot (dR dz) \cdot 2 = 0 \quad (7.2.4)$$

Note that the pressure p applies everywhere on the surface of the element and is therefore subtracted from the active stress σ_θ . From equation (7.2.4), using equation (7.2.3), we obtain

$$\frac{dp}{dR} = - \frac{\sigma \cos^2 \alpha}{R} \quad (7.2.5)$$

Equilibrium of the element shown in Fig. 7.5b implies

$$dp \cdot (\pi R^2) + (\sigma_z + p) \cdot (2\pi R dR) = 0 \quad (7.2.6)$$

from which, using equation (7.2.3), we obtain

$$\frac{1}{2} \frac{dp}{dR} = - \frac{\sigma \sin^2 \alpha}{R} \quad (7.2.7)$$

Summation of equations (7.2.5) and (7.2.7) yields

$$\frac{dp}{dR} = -\frac{2\sigma}{3R} \quad (7.2.8)$$

This equation is integrated from $R = r_i$ to $R = r_o$. Let V_w denote the volume of the ventricle wall and V_{lv} the volume of the ventricle cavity. Then the result of the integration is

$$p_o - p_i = -\frac{2}{3}\sigma \ln \left(\frac{r_o}{r_i} \right) = -\frac{1}{3}\sigma \ln \left(\frac{\pi r_o^2 L}{\pi r_i^2 L} \right) = -\frac{1}{3}\sigma \ln \left(\frac{V_{lv} + V_w}{V_{lv}} \right) \Rightarrow$$

$$\frac{p_{lv}}{\sigma} = \frac{1}{3} \ln \left(1 + \frac{V_w}{V_{lv}} \right) \quad (7.2.9)$$

where $p_{lv} = p_i - p_o$ is the pressure in the left ventricle.

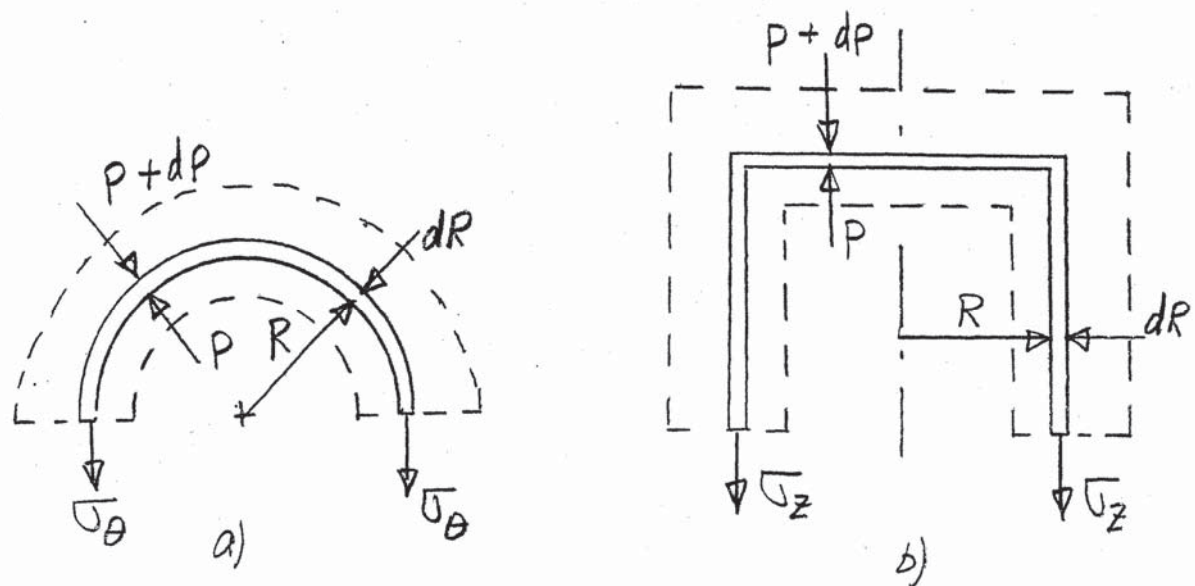


Fig. 7.5

7.2.3 THE ELLIPSOIDAL MODEL

An ellipsoidal model of the left ventricle has been proposed in a paper by Rabben et al. [3]. The following is short outline of this model. For more details the paper should be consulted. Figure 7.1 shows the proposed geometry. The middle surface of the thick-walled shell modelling the ventricle is an axisymmetric ellipsoid. The curvilinear coordinates describing the shell are denoted u , v , and w . The coordinate lines for u are circles, for v are ellipses, and for w are straight lines perpendicular to the middle surface. The following assumptions are made:

1. The surfaces $w = \text{constants}$ are isobars, i.e. surfaces of constant intra-myocardial pressure.
2. The u -lines and v -lines are along the principal curvature directions.
3. The w -coordinate is normal to the isobars.
4. The muscle fiber coincide with the isobars.

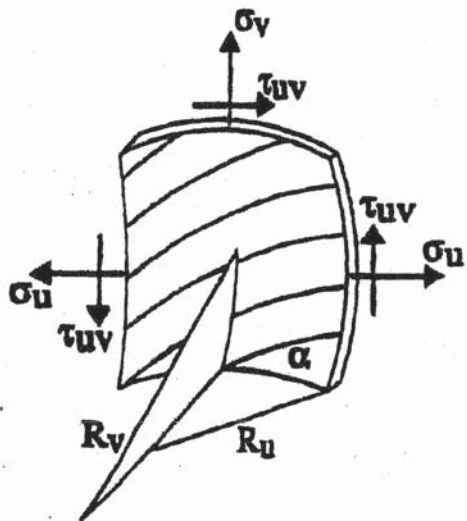


Fig. 7.6 Shell element of thickness dw with stresses.

Figure 7.6 shows a shell element of thickness dw subjected to the normal stresses σ_u and σ_v and the shear stress τ_{uv} , and the pressures p and $p + dp$. The pressures are not shown in Figure 7.6. From equation (7.2.2) we may write for the stresses, not including the pressure p ,

$$\sigma_u = \sigma \sin^2 \alpha, \quad \sigma_v = \sigma \cos^2 \alpha, \quad \tau_{uv} = \sigma \sin \alpha \cos \alpha \quad (7.2.10)$$

where α is the fiber angle, i.e. the angle between the fiber and the equatorial xy -plane. It follows that

$$\sigma_u + \sigma_v = \sigma \quad (7.2.11)$$

Using Laplace's law (2.4.18), we may write

$$-\frac{dp}{dw} = \frac{\sigma_u}{R_u} + \frac{\sigma_v}{R_v} \quad (7.2.12)$$

The equilibrium equation in the z -direction yields, after some calculations,

$$-\frac{dp}{dw} = \frac{2\sigma_v}{R_u} \quad (7.2.13)$$

From the equations (7.2.11-13) we obtain the result

$$-\frac{dp}{dw} = \frac{2\sigma}{R_u(3 - R_u/R_v)} \quad (7.2.14)$$

The fiber angle α has now been eliminated from the model. At the apex the two principal curvatures are equal: $R_u = R_v$, and equation (7.2.14) yields

$$-\frac{dp}{dw} = \frac{\sigma}{R_u} \quad (7.2.15)$$

We assume that the fiber layers are parallel to the middle surface, $w = 0$, where $R_u = R_{mu}$ and $R_v = R_{mv}$. Then we may write

$$R_u = R_{mu} + w, \quad R_v = R_{mv} + w, \quad -\frac{h}{2} \leq w \leq \frac{h}{2} \quad (7.2.16)$$

Integration of equation (7.2.14) through the thickness of the wall results in an expression for the fiber stress

$$\sigma = p_{lv} \left[\frac{2}{3} \ln \left(\frac{R_{mu} + h/2}{R_{mu} - h/2} \right) + \frac{1}{3} \ln \left(\frac{3R_{mv} - R_\mu + h}{R_{mv} - R_\mu - h} \right) \right]^{-1} \quad (7.2.17)$$

This formula may be used to compute the fiber stress when the left ventricular pressure p_{lv} and the geometrical parameters R_{mu} , R_{mv} and h are known.

Example 7.1

To imitate an adult human left ventricle we choose $V_w = 100 \text{ mL}$ and $a_m/b_m = 0.5$. Figure 7.7 shows σ/p_{lv} as a function of V_{lv}/V_w in the range [0.01 - 1.0]. Here σ is: 1) the average fiber stress between equator and apex, 2) the equatorial fiber stress, and 3) the apical fiber stress, all obtained from equation(7.2.17), and 4) the average fiber stress from the Arts' model (7.2.9). We observe that there is very little difference between the four stress curves.

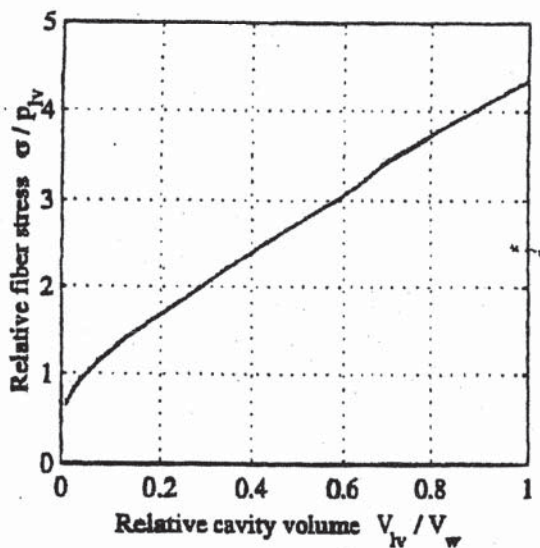


Fig. 7.7 Fiber stress as function of the left ventricular volume.

7.2.4 THE MUSCLE FIBER DIRECTION IN THE ELLIPSOIDAL MODEL

Substitution of the stresses from equation (7.2.10) into equation (7.2.12) yields

$$-\frac{dp}{dw} = \frac{\sigma \cos^2\alpha}{R_{mu} + w} + \frac{\sigma \sin^2\alpha}{R_{mv} + w} \quad (7.2.18)$$

Integration of this equation through the thickness and equating the left ventricle pressure to the one obtained from equation (7.2.17) results in the following constraint on the function $\alpha(w)$

$$\int_{-h/2}^{h/2} \left[\frac{\cos^2\alpha}{R_{mu} + w} + \frac{\sin^2\alpha}{R_{mv} + w} \right] dw = 1 \quad (7.2.19)$$

Another constraint is provided by the condition of moment equilibrium about the z-axis.

$$\int_{-h/2}^{h/2} (\tau_{uv} \cdot r) \cdot 2\pi r dw = 0 \Rightarrow \int_{-h/2}^{h/2} \sin 2\alpha (R_{mu} + w)^2 dw = 0 \quad (7.2.20)$$

Two functions for have been used to estimate the fiber angel variations

$$\alpha = -\mu w + \alpha_m \quad (7.2.21)$$

$$\alpha = -\frac{\pi}{2} \arcsin(2w/h) + \alpha_m \quad (7.2.22)$$

Using the following end-systolic dimensions suggested by a morphological study of Streeter [4]: $h = 12$ mm, $R_{mu} = 20$ mm, and $R_{mv} = 92$ mm, and the constraints provided by equations (7.2.19) and (7.2.20), we obtain the graphs shown in figure 7.2b.

References

- [1] Arts T, Bovendeerd PHM, Prinzen PW, Reneman RS: Relation between left ventricular cavity pressure and volume and systolic fiber stress and strain in the wall. Biophys. J. 1991, v. 59, p. 93-102.
- [2] Chadwick RS: Mechanics of the left ventricle. Biophys. J. 1982, v. 39, p. 279-288.
- [3] Rabben SI, Irgens F, Angelsen B: Equations for estimating muscle fiber stress in the left ventricular wall. Heart and Vessels 1999, v. 14 (4), p. 189-196.
- [4] Streeter DD, Vaishnav RN, Patel DP, Spotnitz HM, Ross J, Sonnenblick EH: Stress distribution in the canine left ventricle during diastole and systole. Biophys. J. 1970, v. 10, p. 345-363